Proceedings of the 2019 Hypervelocity Impact Symposium
HVIS2019
April 14-19, 2019, Destin, FL, USA
HVIS2019-017

Extended Abstract[+]

Mesoscale modeling and debris generation in hypervelocity impacts

Stephanie N. Q. Bouchey* and Jeromy T. Hollenshead

Sandia National Laboratories, PO Box 5800 Mail Stop 1185, Albuquerque, NM 87185-1185
SAND2019-5602 A

1. Introduction

Material fragmentation after a hypervelocity impact is of interest to predictive electro-optical and infrared (EO/IR) modeling. Successful comparisons with data require that submicron fragments are generated in such impacts; however, experimental data has so far been unable to produce fragments of this scale [e.g., 1-3]. This effort investigated the generation of predicted debris from hypervelocity impact of a sphere on a flat, semi-infinite plate. It is hypothesized that explicit modeling of grains, especially in the presence of void and varying grain properties, may lead to differences in predicted strain rates (locally higher) associated with the grain boundaries. Such an effect may lead to smaller predicted fragments sizes than when using the traditional bulk modeling approach and may provide improved understanding of fragmentation modeling in hypervelocity impacts. Comparisons of predicted strain rates at failure (a proxy for fragment size) and material temperature were made between simulations run using a bulk modeling approach and a mesoscale grain modeling approach.

2. Input development

Computational modeling was performed at Sandia National Laboratories using the shock physics analysis package, CTH [4-5]. The current investigation was based on a two-dimensional (2D) description of the problem and was comprised of two suites of simulations. The first suite tested the standard bulk (isotropic, homogeneous) structure and was the nominal case with which to compare the results of the second study, which explicitly modeled mesoscale grains. The nominal problem design was an aluminum sphere impacting a semi-infinite, flat aluminum plate target at a velocity of 4 km/s. Each material was modeled with the SESAME equation of state, a Johnson-Cook strength model, a Johnson-Cook fracture model, and a Grady-Kipp fragmentation model.

Although the bulk model was developed first, many of the system characteristics (e.g. resolution, problem geometry) were driven by the expected requirements for the mesoscale model. High resolution through the grains necessitated exceptionally small simulation domains in order to incorporate the sphere-on-plate geometry. Additionally, the target was designed to be much larger than the projectile to mitigate edge and boundary effects. The projectile was nominally 7 mm in diameter (500 grains across), and the total target area was 2.1 cm wide by 4.1 cm deep. To fill the entire target area with grains would be prohibitively expensive. Thus, a smaller "grains region" of the target was modeled to be 3.5 mm thick and 7 mm wide (14 mm wide when mirrored about the axis). In the bulk model, this small target area was modeled as a single material that matched the material properties of the larger surrounding target matrix area. In both cases, the target matrix area was modeled with a single, bulk material.

+ Full paper can found at https://www.sciencedirect.com/journal/international-journal-of-impact-engineering/special-issue/10MTGP5W4VJ
* Corresponding author. Tel.: +1-505-284-8128.
E-mail address: snquint@sandia.gov.

Traditional model descriptions within CTH are typically macro-scale and do not include any explicit grain structure representation. Consequently, a procedure was necessary to model and initialize grains within CTH. A MATLAB Monte Carlo simulation of 2D grain growth using a Q-state Potts model generated a unit cell of grains. The current configuration allows for eight different grain types in both the target and projectile (16 total materials). Each grain type was randomly distributed within the unit cell, and the entire cell was then scaled such that the average grain size was ~14 μm in diameter. The 14 μm size was estimated from Nakai and Itoh [6], based on the short axis of a characteristic aluminum grain. Finally, this scaled unit cell was tiled repeatedly to generate the impact geometry (projectile and target grains areas), and the result was written out pixel by pixel in a form (diatom) that could be read by CTH.

3. Bulk model

The bulk model suite simulated a projectile striking a target within a larger target matrix. This model suite enabled the following studies: resolution, impact velocity, projectile size, and projectile shape. A custom post-processing script produced histograms and cumulative distribution functions (CDFs) for strain rate at failure and material temperature. For brevity, only histograms will be shown here.

First, an appropriate resolution needed to be defined. For the resolution study, a single projectile size was evaluated across a range of resolutions from 0.875 to 14.0 μm at the nominal impact velocity of 4 km/s. Convergence occurred for material temperature but not the strain rate at failure. This result is not surprising as the Grady-Kipp model used here is dependent on resolution. Rise time of the initial peak in strain rate histograms was chosen as an indication of convergence. Based on these results, the 3.5 μm was chosen as an acceptable mesh resolution.

Next, the projectile size study assessed the effects of projectile curvature and overall size relative to the domain. Histograms and CDFs were evaluated at equivalent times for each model. The histogram plots for strain rate at failure and temperature are shown in Fig. 1 for the projectile. Material temperature was similar between all projectile sizes and appears to be related to geometry scaling. Conversely, strain rate at failure varied significantly between projectile sizes, with smaller projectiles manifesting higher strain rates. In the projectile, the histogram of strain rate at failure exhibited a bimodal shape. The distance between the peaks in each strain rate histogram appears to be at least partially driven by transit time across the object (i.e., by a characteristic length scale, which is projectile diameter in this case). Strain rate at failure was also recorded in the semi-infinite target. There, the strong bimodality seen in the projectile was absent, which suggests that the bimodality may be due primarily to projectile shape. In both the projectile and target, however, onset of the strain rate histogram was related to projectile size.

Three additional simulations tested projectile shape by impacting a cube (face-on), rather than a sphere, into the target at 4 km/s. Results for the projectile are shown in Fig. 2. The lack of bimodality in Fig. 2a is evidence that bimodality is a product of projectile curvature (as was suggested in the previous projectile size study). A more step-like strain rate at failure histogram was apparent, especially in the larger cube impacts. The size of the cube, however, did not influence temperature; this result was also seen in the sphere impacts.

A final set of bulk model simulations explored the effect of increasing impact velocity from the nominal 4 km/s to 6 km/s. This impact velocity increase resulted in a shift to higher strain rates and temperatures, but overall shape and bimodality (in the projectile) were not significantly affected. Impact velocity clearly controls temperature in the projectile, although temperature histograms were nearly unchanged by projectile size for impacts at the same speed.

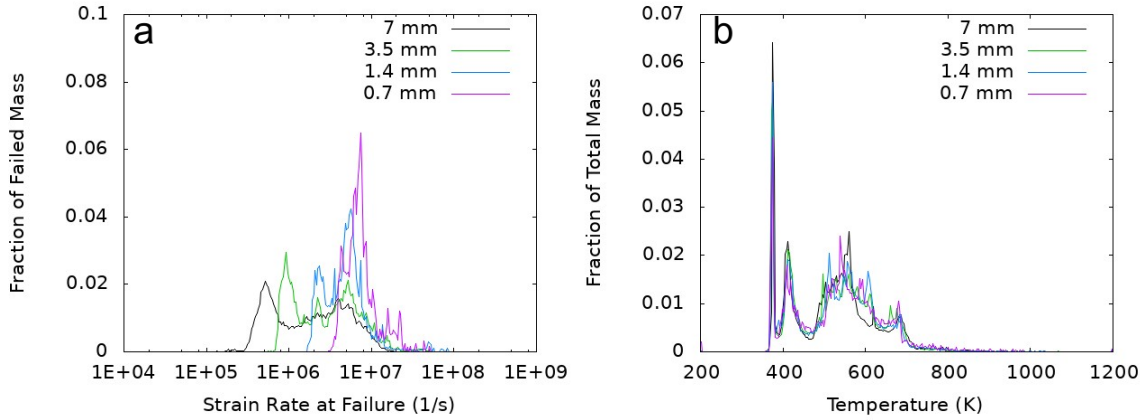

Fig. 1. Projectile size study results. Histograms for (a) strain rate at failure and (b) material temperature for a sphere impacting at 4 km/s.

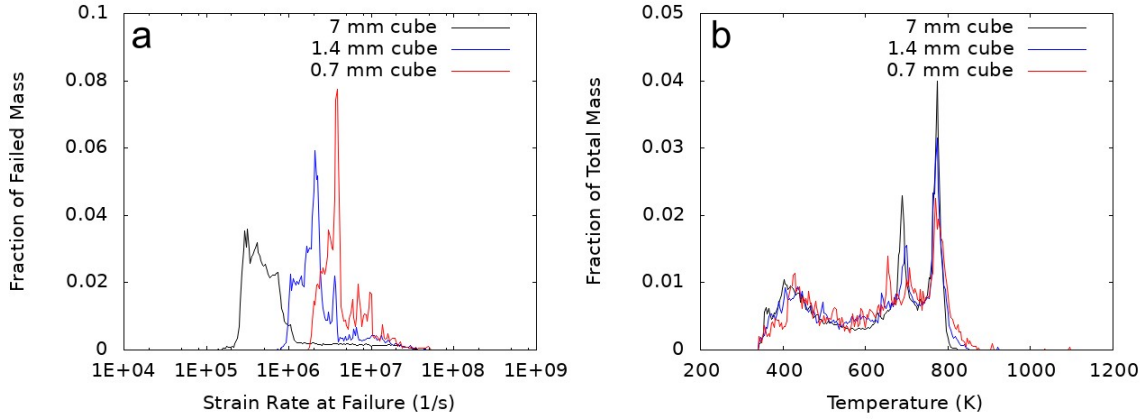

Fig. 2. Projectile shape study results. Histograms for (a) strain rate at failure and (b) material temperature for a face-on cube impacting at 4 km/s.

4. Mesoscale model

In the mesoscale model, the projectile and "grains region" of the target were filled with individual grains, which were described in CTH as separate materials. Eight grain types were randomly distributed through the projectile by the tile method described in Section 2. Similarly, eight (separate) grain types were randomly distributed and tiled through the target grains region. The surrounding target matrix was defined as a single, bulk material. This modeling approach enabled the following studies: fracture strength distribution, yield strength distribution, and porosity. Because each grain type is a separate material, a separate histogram and CDF was produced for each grain type. The histograms/CDF results of each grain type were then averaged for ease of comparison with the isotropic simulation. An initial "consistency case" where all grain types were the modeled as the same material produced the closest approximation to the bulk simulations and served as the standard of comparison for the rest of the simulations (Fig. 3, black line).

The first deviation from the consistency case modified fracture strength. Aluminum alloys vary in fracture strength, and so to simulate this variation in the mesoscale model, a normal distribution of plausible fracture strengths, centered on the fracture strength of Aluminum 1100 was applied to the grains in both the projectile and the target. Results for this study can be found for the projectile in Fig. 3 (green line). An increase in the lowest strain rates compared to the grains consistency result was observed, but the amount of material at higher strain raters remained similar between the two tests. Additionally, temperature remained largely unchanged between the fracture study results and the consistency result.

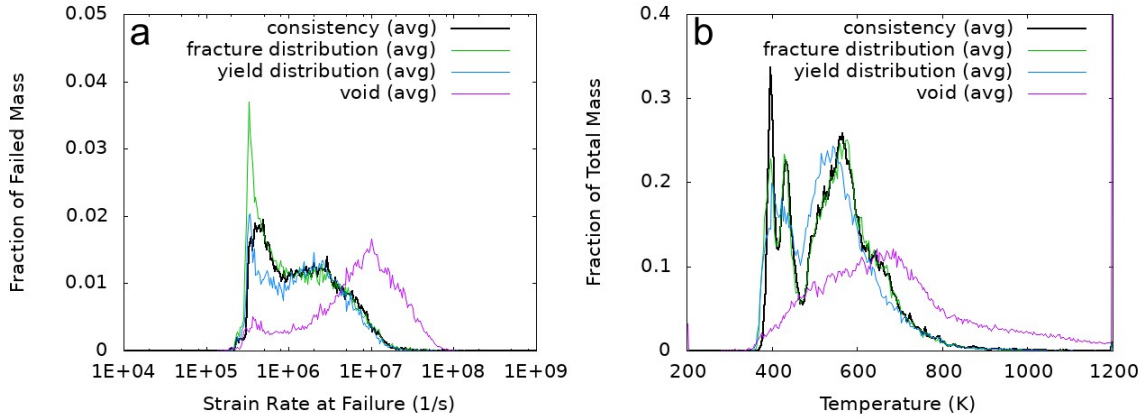

Fig. 3. Summary of mesoscale study results. Histograms for (a) strain rate at failure and (b) material temperature for a sphere impacting at 4 km/s. The insertion of material interfaces (through void) drastically increases strain rate at failure and material temperature.

Another important material property is yield strength. In a process similar to that described above, a distribution of reasonable yield strength values for aluminum was determined by varying parameters in the Johnson-Cook strength equation [7-8]. This distribution was then incorporated into the grain-type materials of both the target and the projectile. Results indicate that changing the strength of the grains reduced the amount of lower strain rates of failure that were produced, but it did not have a substantial effect on higher strain rates at failure or material temperature (Fig. 3, blue line).

Finally, the last suite of simulations explored the role of porosity (void space) in the grain structure. To test the upper bounds of porosity effects, all grains of a single grain-type were removed from the calculation. The resulting void space caused interfaces between grains that allowed several sets of shock and rarefaction waves to pass through the grains. Such behavior dampened the overall shockwave but resulted in locally higher strain rates at failure and material temperatures. This local increase in both parameters resulted in substantial deviation from the grains consistency study (Fig. 3, purple line). The strain rate at failure histogram nearly lost its bimodal shape in the projectile and shifted to higher strain rates in both the projectile and the target. This shift indicates that the projectile size was no longer the dominant property controlling the strain rate at failure. Instead, individual grains became more important.

5. Summary

This work compared the effects of modeling grain structure in hypervelocity impact simulations. Comparisons of strain rate at failure (fragment size) and material temperature were made between a suite of simulations performed with the standard bulk modeling structure and one in which individual grains were modeled. Smaller fragments or higher temperatures are needed to match EO/IR signatures from observed impacts. Results from the various studies described herein indicate that strain rate at failure is influenced primarily by projectile size, impact velocity, and material porosity. Material temperature is predominantly influenced by impact velocity and porosity; not by projectile size. Changes to the material properties within grains tended to affect lower strain rates only, but material interfaces (here, manifested as material porosity) drastically increased strain rate at failure and material temperatures. Higher strain rates are likely to produce smaller debris fragments, which, along with hot debris may help provide evidence supporting the generation of sub-micron fragments currently required by many EO/IR predictive models to successfully compare with observed hypervelocity impacts. Future work will focus on extending the study to three dimensions, assessing more realistic grain aspect ratios, and simulating other types of interfaces such as inclusions and dislocations.

Acknowledgements

The authors wish to thank Torch Technologies (specifically Jim Burke, Steven Henke, and Karen Hirsch) for supporting this work. This paper describes objective technical results and analysis. Any subjective views or opinions that might be expressed in

the paper do not necessarily represent the views of the U.S. Department of Energy or the United States Government. Sandia National Laboratories is a multimission laboratory managed and operated by National Technology & Engineering Solutions of Sandia, LLC, a wholly owned subsidiary of Honeywell International Inc., for the U.S. Department of Energy's National Nuclear Security Administration under contract DE-NA0003525.

References

[1] Glenn, L. A. and Chudnovsky, A., 1986. Strain-energy effects on dynamic fragmentation, Journal of Applied Physics, vol. 59, no. 4, p. 1379.
[2] Grady, D. E. and Kipp, M. E., 1997. Fragmentation properties of metals, International Journal of Impact Engineering, vol. 20, no. 1-5, pp. 293-308.
[3] Grady, D. E., 2008. Fragment size distributions from the dynamic fragmentation of brittle solids, International Journal of Impact Engineering, vol. 35, no. 12, pp. 1557-1562.
[4] McGlaun, J.M., Thompson, S.L., Elrick, M.G., 1990. CTH: A Three-Dimensional Shock Wave Physics Code, International Journal of Impact Engineering, 10(1-4), pp. 351-360.
[5] Hertel, E.S. Bell, R.L., Elrick, M.G., Farnsworth, A.V., Kerley, G.I., McGlaun, J.M., Petney, S.V., Silling, S.A., Taylor, P.A., Yarrington, L., 1993. "CTH: A Software Family for Multi-Dimensional Shock Physics Analysis," Proceedings of the 19th International Symposium on Shock Waves, pp. 377-382.
[6] Nakai, M., Itoh, G., 2014. The Effect of Microstructure on Mechanical Properties of Forged 6061 Aluminum Alloy, Materials Transactions 55, pp. 114-119.
[7] Johnson, G.R., Cook, W.H., 1983. "A Constitutive Model and Data for Metals Subjected to Large Strains, High Strain Rates and High Temperatures," Seventh International Symposium on Ballistics, The Hague, Netherlands.
[8] Silling, S.A., 1996. "CTH Reference Manual: Viscoplastic Models," SAND91-0292, Sandia National Laboratories, Albuquerque, NM.